Available online at www.sciencedirect.com
ScienceDirect
Geochimica et Cosmochimica Acta 71 (2007) 2896–2905
Geochimica et Cosmochimica Acta
www.elsevier.com/locate/gca

Monazite, iron oxide and barite exsolutions in apatite aggregates from CCSD drillhole eclogites and their geological implications

Xiaoming Sun [a,b,*], Qian Tang [a], Weidong Sun [b,f], Li Xu [a], Wei Zhai [a], Jinlong Liang [a], Yeheng Liang [a], Kun Shen [c], Zeming Zhang [d], Bing Zhou [b,e], Fangyue Wang [b,e]

[a] *Earth Sciences Department of Sun Yatsen University, Guangzhou 510275, China*
[b] *Key Laboratory of Isotope Geochronology and Geochemistry, Guangzhou Institute of Geochemistry, Chinese Academy of Sciences, Guangzhou 510640, China*
[c] *Geological Institute of Shandong Province, Jinan 250013, China*
[d] *Institute of Geology, Chinese Academy of Geological Sciences, Beijing 100037, China*
[e] *State Key Laboratory of Continental Dynamics, Department of Geology, Northwest University, Xi'An 710069, China*
[f] *Department of Earth and Space Sciences, University of Science and Technology of China, Hefei 230026, PR China*

Received 20 November 2006; accepted in revised form 26 March 2007; available online 12 April 2007

Abstract

We have identified abundant exsolutions in apatite aggregates from eclogitic drillhole samples of the Chinese Continental Scientific Drilling (CCSD) project. Electron microscope and laser Raman spectroscopy analyses show that the apatite is fluorapatite, whereas exsolutions that can be classified into four types: (A) platy to rhombic monazite exsolutions; (B) needle-like hematite exsolutions; (C) irregular magnetite and hematite intergrowths; and (D) needle-like strontian barite exsolutions. The widths and lengths of type A monazite exsolutions range from about 6–10 μm (mostly 6 μm) and about 50–75 μm, respectively. Type B exsolutions are parallel with the *C* axis of apatite, with widths ranging from 0.5 to 2 μm, with most around 1.5 μm, and lengths that vary dramatically from 6 to 50 μm. Type C exsolutions are also parallel with the *C* axis of apatite, with lengths of ~30–150 μm and widths of ~10 to 50 μm. Type D strontian barite exsolutions coexist mostly with type B hematite exsolutions, with widths of about 9 μm and lengths of about 60–70 μm. Exsolutions of types B, C and D have never been reported in apatites before. Most of the exsolutions are parallel with the *C* axis of apatite, implying that they were probably exsolved at roughly the same time. Dating by the chemical Th–U-total Pb isochron method (CHIME) yields an U–Pb isochron age of 202 ± 28 Ma for monazite exsolutions, suggesting that these exsolutions were formed during recrystallization and retrograde metamorphism of the exhumed ultrahigh pressure (UHP) rocks. Quartz veins hosting apatite aggregates were probably formed slightly earlier than 202 Ma. Abundant hematite exsolutions, as well as coexistence of magnetite/hematite and barite/hematite in the apatite, suggest that the oxygen fugacity of apatite aggregates is well above the sulfide-sulfur oxide buffer (SSO). Given that quartz veins host these apatite aggregates, they were probably deposited from SiO_2-rich hydrous fluids formed during retrogression of the subducted slab. Such SiO_2-rich hydrous fluids may act as an oxidizing agent, a feasible explanation for the high oxygen fugacity in convergent margin systems.

* Corresponding author. Fax: +86 20 84110968.
E-mail address: eessxm@mail.sysu.edu.cn (X. Sun).

0016-7037/$ - see front matter © 2007 Elsevier Ltd. All rights reserved.
doi:10.1016/j.gca.2007.03.030

1. INTRODUCTION

Mantle wedges above the subduction zone, and consequently arc magmas, are usually considerably more oxidized compared to mid-ocean ridge basalts (MORB) and ocean island basalts (OIB) (Ballhaus, 1993; Brandon and Draper, 1996; Parkinson and Arculus, 1999; Mungall, 2002; Sun et al., 2004b). Given that high oxygen fugacity is very important for Cu, Au ore genesis (Sillitoe, 1997; Mungall, 2002; Sun et al., 2004a; Liang et al., 2006), the mechanism that leads to oxidizing convergent margin systems is of wide interest. It is generally agreed that the high oxygen fugacity in the mantle wedge and arc magmas are due to the addition of subduction-released oxidizing fluids or melts (Brandon and Draper, 1996; Luhr and Aranda-Gomez, 1997; Parkinson and Arculus, 1999).

In general, C, H, S and Fe are elements, which are present in sufficient abundance and have variable oxidation states in the mantle, necessary to influence the redox states of the mantle (Mungall, 2002). Of the four elements, carbon and sulfur play very minor roles in oxidizing mantle rocks to oxygen fugacities above the SSO buffer (Brandon and Draper, 1996; Mungall, 2002). Water content is the most obvious difference between convergent margin environments and those for MORB and OIB: both mantle wedges and arc magmas have considerably more water than MORB and OIB due to the recycling of water-rich fluids released from subducting slabs (Wood et al., 1990; Arculus, 1994). The effects of water, however, depend on the physical separation of its decomposition products: H_2 and O_2 (Brandon and Draper, 1996), which is thought to be difficult in the mantle (Mungall, 2002). In contrast, Fe is believed to be the most important redox agent, and the only one that can introduce very high oxygen fugacity into the convergent margin system (Mungall, 2002). It was therefore argued that "if an arc magma has $\log fO_2 >$ SSO buffer, then it must contain a component of melted oceanic crust" (Mungall, 2002).

Here, however, we report abundant oxide exsolutions identified in apatite aggregates from eclogitic drillhole samples from the CCSD, which strongly suggests that solute-rich hydrous fluids can also act as an oxidizing agent that lead to high oxygen fugacity in convergent margin systems (Brandon and Draper, 1996).

2. GEOLOGICAL BACKGROUND AND SAMPLES

The Dabie–Sulu belt is the eastern part of the Qinling–Dabie orogenic belt in central China, which was formed by subduction (Sun et al., 2002c) and consequent collisions between different microplates (Li and Sun, 1996; Li et al., 1996; Zhang et al., 1996; Meng and Zhang, 2000; Sun et al., 2002b), followed by final continental collisions between the South and North China Blocks in the Triassic period (Li et al., 1993; Liou et al., 1996; Sun et al., 2002a,c; Zheng et al., 2003). It is, so far, the largest recognized ultrahigh pressure (UHP) metamorphic belt in the world. Studies show that the whole belt was once subducted down to more than 100 km depths (Xu et al., 1992; Jin et al., 1998; Yang and Jahn, 2000; Ye et al., 2000). Therefore, it has been a hot topic among geoscientists (Liou and Zhang, 1996; Carswell et al., 2000; Li et al., 2000; Ye et al., 2002; Zheng et al., 2004; Xiao et al., 2006).

In order to investigate the evolution of the Qinling–Dabie orogenic belt, the CCSD project was carried out in the southern limb of the Su-Lu ultrahigh-pressure metamorphic terrain in Donghai County of Jiangsu Province (Xu et al., 1998; Xu, 2004; Zhang et al., 2005a) (Fig. 1). The drill core obtained from the main hole of the CCSD consists mainly of eclogites, ortho- and paragneisses, ultramafic rocks, and some schist and quartzite (Zhang et al., 2004, 2005c). The major rock-forming minerals are garnet, omphacite, phengite, quartz and kyanite, and the main accessory minerals are rutile, apatite and paragonite (Zhang et al., 2004). Apatite, which is one of the most common accessory minerals in the CCSD eclogites (Zhang et al., 2005b), is believed to have recorded subduction and exhumation history of the CCSD UHP rocks.

Apatite aggregates with oriented oxide inclusions have been found in many CCSD quartz vein samples (e.g., samples 2005011, 2005038, 2005049, 2003571, 2003588). The apatite samples reported here were collected from the CCSD main drill hole at the depth of 370 m. The sample number is 2003558 (B162R140P1g). The host rock is pyrite- and rutile-bearing quartz eclogite with quartz veins. Apatite occurs as massive aggregates to irregular veins with widths of 2–5 cm in quartz veins (Fig. 2a).

3. ANALYTICAL METHODS

Laser Raman analysis was done at the Guangzhou Institute of Geochemistry with a Renishaw RM 2000 Raman spectrometer with 5 mw of 514 nm Ar laser excitation at room temperature. The beam size for Raman spectroscopy was 2 μm. Electron microprobe and scanning analyses were carried out in the Modern Analytical Center of Sun Yatsen University by using a JXA-8800R electron microprobe with an Oxford inca-300 energy dispersive X-ray spectrometer (EDS). The analytical accelerating voltage was 20 kV. The detection limit of the electron microprobe was 0.2% and resolution of the secondary electron images was 6 nm. Cobalt was used in calibration of peaks of EDS analysis.

CHIME dating of monazite exsolutions was performed by a JXA-8800M electron microprobe in the State Key Laboratory for Mineral Deposits Research at Nanjing University. The monazite grains for CHIME dating were selected under a polarized microscope and observed by a scanning electron microscope in order to avoid inclusions or fractures. UO_2, ThO_2 and Pb-glass were used as standards for U, Th and Pb concentrations. The operating conditions were an accelerating voltage of 20 kV, electricity current of 1×10^{-7} A, and an electron beam diameter of 1 μm. Measuring time and background were 100 and 50 s for U and Th, and 200 and 100 s for Pb. The detection limits for U, Th and Pb were 46, 60 and 46 ppm, respectively.

4. RESULTS

4.1. Mineralogy of oriented mineral inclusions

Electron microprobe analyses show that the apatite is fluorapatite in composition (Fig. 2b). Oriented mineral

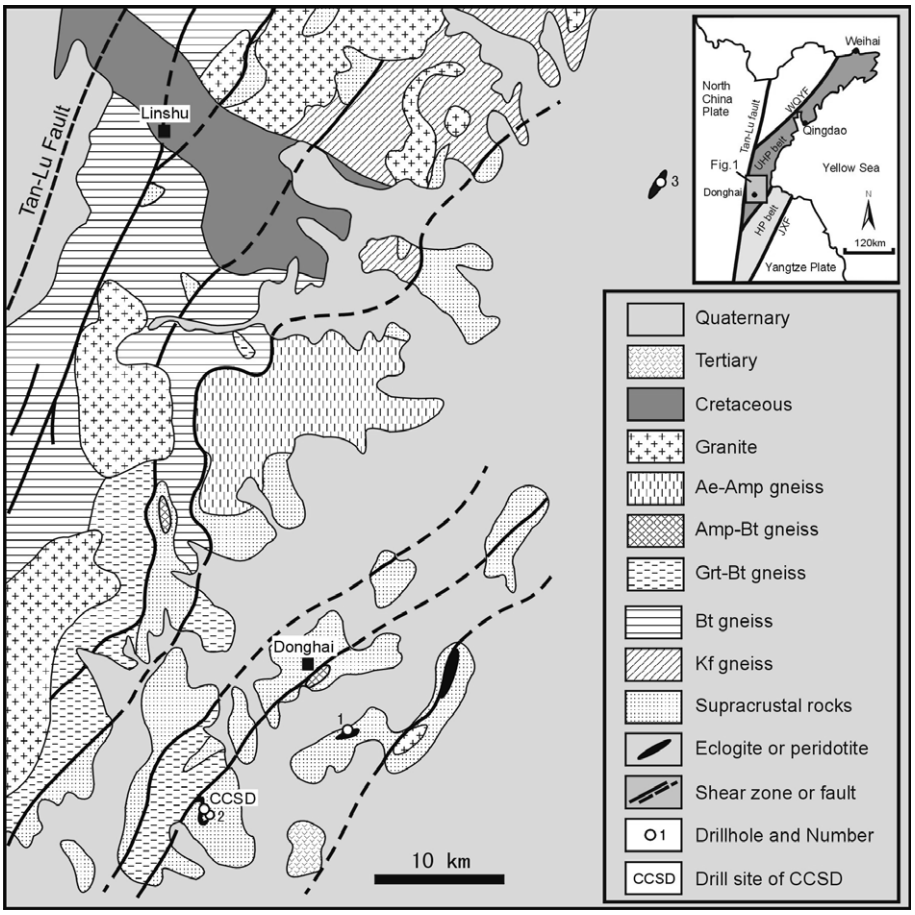

Fig. 1. Sketched geologic map of the Donghai area of the southern Sulu UHP belt, showing the location of the CCSD.

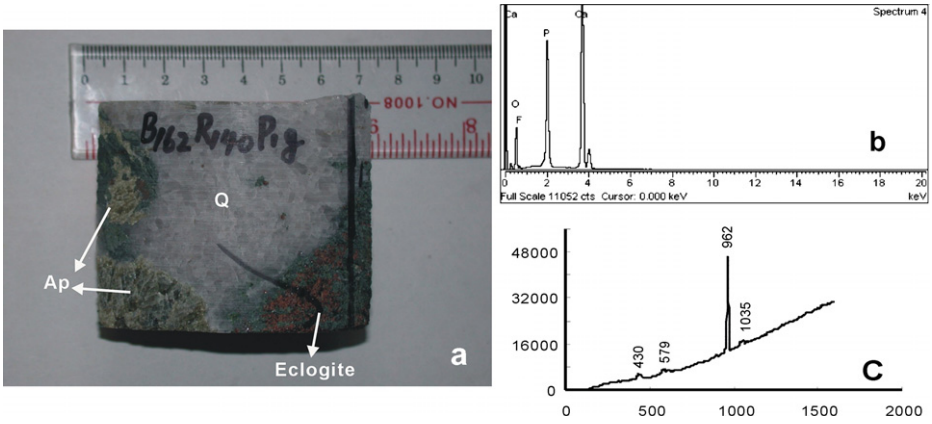

Fig. 2. Apatite aggregates (a) and their energy dispersive X-ray spectrometer (EDS) spectrum (b) and laser Raman spectrum (c) in CCSD eclogite. Ap-apatite; Q-quartz. The peaks at 430, 579, 962 and 1035 cm^{-1} represent apatite.

inclusions in the apatite can be classified into two types: transparent and opaque. The former are usually light yellow-color crystals of 6–10 μm × 50–70 μm in size, and unevenly distributed in apatite. The latter are mostly needle-like to irregular massive crystals. Both transparent and opaque inclusions are oriented needle-like grains, parallelling to the *C* axis of host apatite grains. Through microprobe and laser Raman analyses, we have identified four types of oriented mineral inclusions in apatite:

[A.] Platy to rhombic monazite inclusions, which are mostly elongated parallel to the *C* axis of host apatite, have widths of 6–10 μm and lengths of 50–75 μm (Fig. 3a and b). Electron microprobe analyses

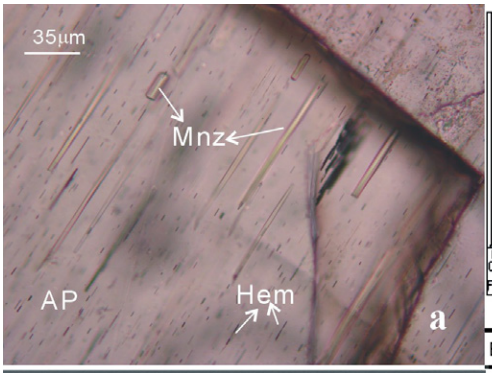

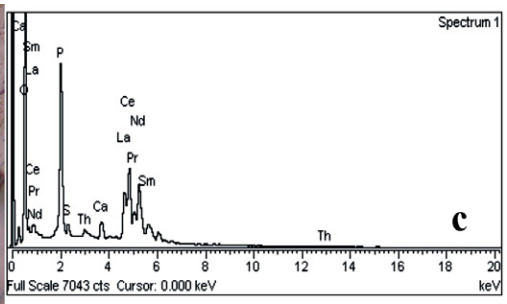

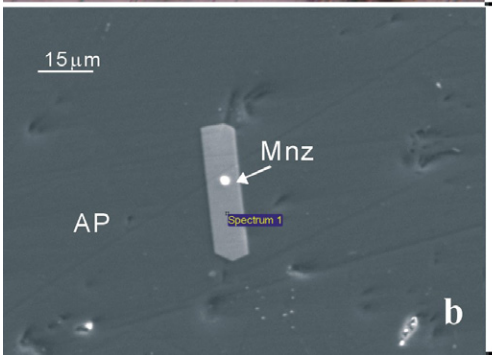

Element	Wt%	Atom%	Oxides	Wt%
P	12.96	15.83	P_2O_5	29.70
S	0.87	1.03	SO_3	2.17
Ca	1.48	1.39	CaO	2.07
La	15.78	4.30	La_2O_3	18.51
Ce	27.22	7.35	Ce_2O_3	31.88
Pr	2.76	0.74	Pr_2O_3	3.23
Nd	8.26	2.17	Nd_2O_3	9.64
Sm	0.85	0.21	Sm_2O_3	0.98
Th	1.60	0.26	ThO_2	1.82
O	28.22	66.72		

Fig. 3. Photomicrographs of oriented monazite inclusions (Type A) taken under microscope (a), BSE image (b), EDS spectrum (c) and chemical composition (3d). The mineral symbols: Mnz-monazite; Ap-apatite; Hem-hematite.

show that the monazites contain P, O, Th, S and high concentrations of light rare earth elements (LREE). The P and O contents as percentages of total atom weight are 15.83 and 66.72%, respectively, with P/O atomic ratios of approximately 1/4, indicating that they are LREE phosphate minerals. The total atomic percentage of LREE is 15.03% and LREE/$PO_4 \approx 1$. Therefore, the Type A inclusions are Th and S bearing monazites with a molecular formula of (LREE)-PO_4. The ThO_2 concentration of this type of monazite is 1.82 wt% (Fig. 3), which is much higher than the usual 0.5% in monazite intergrown with apatite in typical metamorphic rocks (Anderssona et al., 2002).

[B.] Needle-like hematite inclusions, which are also mostly elongated parallel to the *C* axis of host apatite, have widths of only 0.5–2 μm, with most around 1.5 μm, and lengths that vary dramatically from 6 to 50 μm (Fig. 4a). Electron microprobe analyses show that they are MgO-bearing (0.48%) iron oxides. Laser Raman analyses demonstrate that they are hematite with specific peaks of 226, 292, 408 and 653 cm^{-1} (Fig. 4b).

[C.] Irregular magnetite and hematite intergrowths, which occur as massive opaque blebs with length of 30–150 μm and widths of 10–50 μm (Fig. 5a). Electron microprobe analyses show that they are iron oxides with 98.3 wt% Fe_2O_3, 0.66 wt% MgO and 1.04 wt%

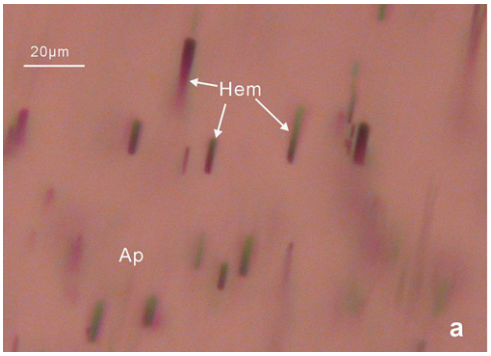

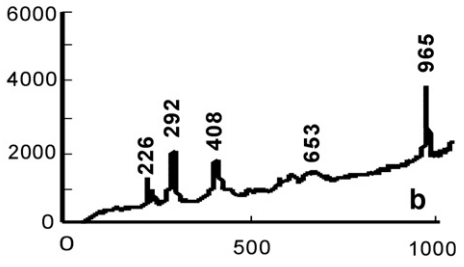

Fig. 4. Photomicrographs of oriented hematite inclusions (Type B) (a) and its laser Raman spectrum (b). The mineral symbols are same as Fig. 3. The peaks at 226, 292, 408 and 653 cm^{-1} in 4b are specific peaks of hematite.

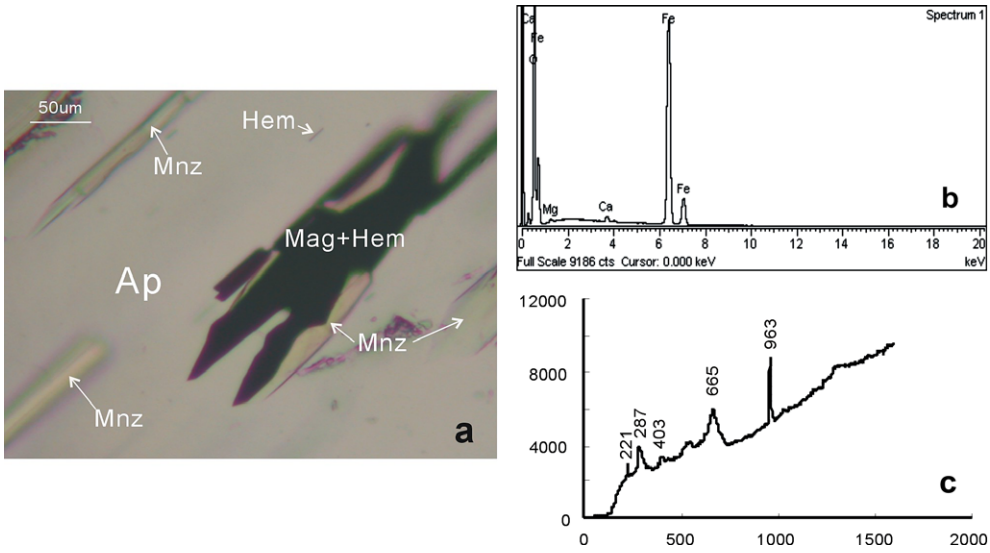

Fig. 5. Photomicrograph of magnetite and hematite intergrowth inclusions (Type C) (a), spectra of EDS (b) and laser Raman spectrum (c). The mineral symbols are same as Fig. 3. Mag-magnetite. The peaks in 5c at 221, 287 and 403 cm^{-1} represent hematite, while the peak at 665 cm^{-1} represents magnetite.

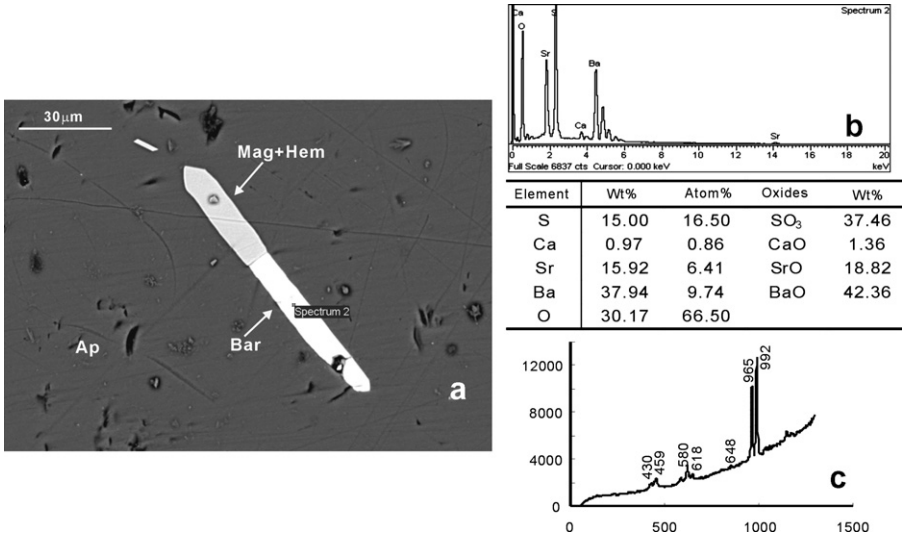

Fig. 6. BSE image of barite inclusion (Type D) (a), EDS spectrum and chemical composition (b) and laser Raman spectrum (c). The peaks at 992, 648, 618 and 459 cm^{-1} in 6d represent barite. The upper part of the need-like inclusions is a magnetite hematite intergrowth identified using laser Raman and electron microprobe analyses.

CaO. Laser Raman analyses demonstrate that they are hematite and magnetite intergrowths, the specific peaks for the former are 221, 287 and 403 cm^{-1}, while that for the latter is 665 cm^{-1}. The high CaO concentration is likely due to signals from the host.

[D.] Needle-like strontian barite inclusions have widths of about 9 μm and lengths of about 60 to 70 μm (Fig. 6a). Electron probe analyses show that they contain S, Sr, Ba, O and a small amount (0.86 wt%) of Ca. The atomic percentages of S and O are 16.5 and 66.5%, respectively, with S/O of about 1:4, confirming that they are sulfate minerals (Fig. 6b). In addition, the total atomic percentages of Ba and Sr together are approximately the same as SO_4. Therefore, the type D mineral inclusions are strontian barite with a molecular formula of (Sr, Ba)SO_4. Laser Raman analyses demonstrate that they are barite with specific peaks at 992, 648, 618 and 459 cm^{-1} (Fig. 6c).

4.2. CHIME dating of the monazite exsolutions

Monazite contains high amounts of radioactive elements, such as U and Th, with negligible common Pb (Williams et al., 1983; Corfu, 1988; Parrish, 1990; Williams and

Jercinovic, 2002), making it a suitable mineral for dating by CHIME (Suzuki and Adachi, 1991, 1998; Montel et al., 1996; Rhede et al., 1996; Cocherie and Albarede, 2001). Although the analytical error of CHIME ($\pm 10 \sim 30$ Ma) is larger than that associated with the sensitive high resolution microprobe (SHRIMP) method, the CHIME method is well-suited for dating monazite grains with a diameter of less than 20 μm, and particularly monazite exsolutions because the electron beam can be adjusted to 1–2 μm.

In this study, 51 monazite inclusions in apatite aggregates were analyzed using an electron microscope. The results are shown in Table 1 and plotted on Fig. 7. The isochron line gives an intercept of 0.0020 ± 0.0025 and a slope of 0.0085 ± 0.001. The isochron age of the monazites is calculated with the CHIME software created by (Suzuki and Adachi, 1991, 1994), yielding a result of 202 ± 28 Ma, MSWD = 2.02.

5. DISCUSSION

For the following reasons, we propose that these oriented needle-like mineral inclusions in apatite formed through exsolution during decompression. First, all the inclusions are oriented roughly parallel to *C* axes of the host apatite. It is difficult to enclose such a large number of tiny minerals arranged in the same direction. Second, the inclusions are very small and needle-like; while their oxygen fugacities are far above those of host eclogites, none of them can survive without protection of apatite. Moreover, all the mineral inclusions are hosted only in apatite, with no inclusions found in any other minerals in the quartz veins. Given that apatite in quartz veins is younger than the host eclogite, it would be very difficult for the inclusions to be selectively captured by apatite.

Apatite has a specific hexagon structure with channels paralleling the *C* axis, and can thus hold a large number of elements with large radius ions under UHP; these elements can then be released during decompression and form exsolutions. Needle-like monazite inclusions in apatite have been found previously in Dabie–Sulu eclogites (Liou et al., 1998; Zhang and Liou, 1999). These authors proposed that the monazite inclusions may have exsolved from host apatite during decompression (Liou et al., 1998; Zhang and Liou, 1999). More recently, both monazite and sulfide (such as pyrrhotite and pyrite) inclusions in apatites from eclogites were attributed to exsolution during decompression (Hong et al., 2003; Zhu and Massonne, 2005). In this study, we found abundant mineral inclusions oriented along crystalgraphic axes in apatite aggregates associated with quartz veins in CCSD eclogites under microscope. Laser Raman and electron microprobe analyses demonstrated that the inclusions were monazite, iron oxides and barite. To our knowledge, this is the first report of iron oxide and barite exsolutions in apatite.

Abundant hematite exsolutions, as well as the coexistence of magnetite/hematite and barite/hematite exsolutions in apatite, suggest that the oxygen fugacity of apatite aggregates is well above the SSO buffer. By contrast, the host rock is pyrite- and rutile-bearing quartz eclogite, which has dramatically lower oxygen fugacity. These facts suggest that the oxidizing components hosted in apatite originated in deeper levels and migrated to the current locations. Given that apatite aggregates are closely associated with quartz veins, these highly oxidizing components were probably closely associated with Si-rich hydrous fluids, which are very common fluids released from subducting slabs.

The origins of the quartz veins in the CCSD samples, and in Dabie–Sulu orogenic belt in general, remain uncertain. Early studies suggested that the quartz veins formed through an influx of later-stage external fluids (Li et al., 2001). Based on the lack of UHP minerals and isotopic data, it was later proposed that the quartz veins did not undergo UHP peak metamorphism, but formed mainly in P-T conditions between UHP and HP metamorphism of eclogites during exhumation of the subducted plate and before recrystallization of HP eclogites (Zheng, 2004), during retrograde metamorphism (Sun et al., 2006; Xu et al., 2006a,b). A recent study, however, reported the occurrence of N_2-CH_4 inclusions in quartz veins in CCSD eclogites, which indicates that at least some quartz veins in CCSD UHP rocks formed quite early and probably underwent UHP metamorphism (Xu et al., 2006a,b). Moreover, the lack of UHP minerals in quartz veins cannot be used to argue that these quartz veins formed at low pressure because, without protection (e.g., as inclusions in zircon or garnet), UHP minerals usually disappear during retrograde metamorphism. In fact, coesite pseudomorphs hosted in garnet and allanite in quartz veins have been found in many different locations, including CCSD samples (Zhai et al., 2005).

For Dabie UHPM rocks, three episodes of eclogite-facies metamorphisms, at 254–239 , 238–230 and 218–206 Ma, respectively, have been identified based on SHRIMP dating and multiphase metamorphic textures and index mineral inclusions within zircon (Liu et al., 2006a,b). Based on evolutional processes and geochronology, Zhang et al. (2005c) established the UHPM P-T-t path of the Dabie–Sulu belt and proposed that this area experienced epidote amphibolite facies prograde metamorphism (stage I), UHPM (stage II), coesite eclogite facies retrograde metamorphism (stage III), quartz eclogite retrograde metamorphism (stage IV), granulite facies retrograde metamorphism (stage V), amphibolite facies retrograde metamorphism (stage VI), epidote amphibolite facies retrograde metamorphism (stage VII), and greenschist facies retrograde metamorphism (stage VIII) (Zhang et al., 2005c). Based on previous results in geochronology and metamorphic petrology, the age of 202 ± 28 Ma for monazite exsolutions in the apatite aggregates implies that the formation of apatites occurred from quartz eclogite retrograde metamorphism (stage IV) to amphibolite facies retrograde metamorphism (stage VI) during exhumation of the subducted plates. The UHPM rocks were raised rapidly from a depth of 100–30 km at a rate of about 4 km/Ma, resulting in a dramatic decline in pressure, coupled with a slow decrease in temperature with a cooling rate of about 8 °C/km, and simultaneous dehydration and decomposition of minerals (Xu et al., 2005; Zhang et al., 2005c). Some of the quartz veins may have formed as a consequence of this process. Overall, retrogression from eclogite to amphibolite metamorphism requires the addition of water. In other

Table 1
Electron microprobe analytical data of monazite exsolutions in apatite aggregates (wt%) and their apparent age (t, Ma)

Analytical No.	ThO_2	UO_2	PbO	Appearance age (t, Ma)	ThO_2^*
1	3.103	0.157	0.027	177.42	3.609
2	2.915	0.171	0.034	232.16	3.469
3	1.901	0.107	0.021	221.4	2.247
4	3.121	0.2	0.028	176.34	3.766
5	1.992	0.082	0.02	210.01	2.257
6	2.645	0.189	0.035	254.3	3.258
7	1.097	0.066	0.014	252.79	1.311
8	2.683	0.137	0.029	219.78	3.126
9	1.129	0.082	0.013	220.89	1.394
10	2.962	0.178	0.032	214.34	3.538
11	2.055	0.14	0.026	245.38	2.509
12	2.073	0.103	0.023	226.41	2.406
13	1.179	0.092	0.015	240.48	1.477
14	1.737	0.152	0.019	202.12	2.228
15	1.379	0.063	0.013	194.76	1.582
16	1.431	0.098	0.021	283.93	1.75
17	2.583	0.139	0.025	195.48	3.032
18	1.388	0.074	0.012	174.98	1.627
19	1.98	0.073	0.017	181.97	2.215
20	2.078	0.113	0.029	280.56	2.445
21	2.036	0.142	0.034	321.54	2.499
22	1.938	0.132	0.018	180.59	2.364
23	4.798	0.363	0.048	190.63	5.97
24	2.798	0.111	0.031	232.54	3.157
25	1.899	0.094	0.019	204.44	2.203
26	1.641	0.269	0.024	226.36	2.512
27	2.342	0.103	0.024	212.6	2.675
28	2.269	0.091	0.024	221.81	2.563
29	2.537	0.127	0.032	256.85	2.949
30	3.689	0.214	0.047	253.84	4.383
31	2.293	0.102	0.022	198.86	2.622
32	2.581	0.108	0.034	274.39	2.932
33	2.553	0.099	0.029	238.98	2.874
34	1.912	0.106	0.022	231.06	2.255
35	4.285	0.252	0.05	232.16	5.101
36	1.979	0.127	0.022	218.12	2.39
37	1.259	0.06	0.017	276.63	1.454
38	2.14	0.107	0.026	247.53	2.487
39	2.547	0.13	0.032	255.16	2.969
40	1.962	0.09	0.018	189.47	2.252
41	1.431	0.105	0.021	280.32	1.772
42	1.007	0.072	0.013	248.13	1.24
43	1.897	0.122	0.022	227.38	2.292
44	1.191	0.08	0.013	212.53	1.45
45	1.642	0.099	0.023	277.11	1.964
46	1.282	0.103	0.019	278.04	1.617
47	1.149	0.085	0.016	265.73	1.425
48	1.528	0.092	0.02	259.18	1.826
49	1.54	0.1	0.018	228.77	1.864
50	1.73	0.132	0.024	263.16	2.158
51	1.483	0.257	0.021	215.03	2.314

Note. $ThO_2^* = ThO_2 + \frac{UO_2 \times W_{Th}}{W_U\{\exp(\lambda_{232}t)-1\}} \times \{\frac{\exp(\lambda_{232}t)+137.88\exp(\lambda_{238}t)}{1}38.88 - 1\}$, where W is molecular weight of each oxides, $W_{Th} = 264$, $W_U = 270$. Monazite contains high Th and its radiogenic Pb is mainly ^{208}Pb, thus $W_{Pb} = 224$. Radioactive decay constants (λ) of ^{232}Th, ^{238}U and ^{235}U are 4.9475×10^{-11} a^{-1}, 1.55125×10^{-10} a^{-1} and 9.848×10^{-10} a^{-1}, respectively.

words, the whole retrograde metamorphism process usually forms more hydrous minerals than those being decomposed. In contrast, hydrous fluids released from subducting slabs are usually Si-rich. Therefore, no matter what pressure the quartz veins formed at, the source materials were supplied through subduction.

We propose that apatite aggregates were probably formed at very high pressures, so that they contained high concentrations of oxides, and exsolutions occurred when pressure diminished during retrograde metamorphism. Impurity elements incorporated in apatite at high pressure became unstable and were expelled from the

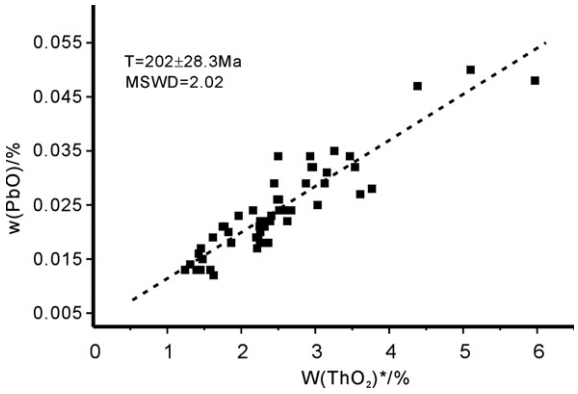

Fig. 7. Plot of ThO_2* vs. PbO for monazite inclusions in apatite.

host minerals. Combination of the expelled LREE with P produced monazite exsolutions, while Sr and S combined to form stronian barite, and iron oxide formed magnetite and hematite.

Considering that apatite aggregates with oriented oxide inclusions have been found in many CCSD samples (e.g., samples 2005011, 2005038, 2005049, 2003571, 2003588), the appearance of apatite aggregates with a large amount of iron oxides and sulfates in the CCSD quartz veins suggests the formation of highly oxidizing SiO_2-rich hydrous fluids during the subduction process. This kind of fluid is very likely to have contributed to the generation of high oxygen fugacity in convergent margin systems, mantle wedges, and arc magmas. These highly oxidizing components suggest that a slab-derived melt is not always necessary to produce arc magmas with high oxygen fugacity (above the SSO buffer). Highly oxidizing hydrous fluids may have played a more important role than previously recognized.

Note that the host eclogites are much more reducing compared to fluids, so a considerable amount of oxidizing components in fluids might have been lost through interactions with the wall rocks during ascent, resulting in the preservation of only the oxidizing components enclosed in apatite aggregates.

6. CONCLUSIONS

Apatite aggregates in quartz veins from CCSD drill hole samples were most likely formed through deposition of slab-derived Si-rich fluids. Abundant hematite exsolutions, as well as the coexistence of magnetite/hematite and barite/hematite assemblages in apatite, show that the oxygen fugacity of apatite aggregates is well above the SSO buffer. Consequently, slab-derived fluids can be highly oxidizing. This kind of fluid is very likely one of the efficient agents that caused the high oxygen fugacity in convergent margin systems.

ACKNOWLEDGMENTS

This work is jointly supported by Natural Science Foundation of China (NSFC) (No. 40399142, 40525010), CAS Key Laboratory of Isotope Geochronology and Geochemistry (No. GIGIso-0504), National Key Basic Research Development Program (973 project) (No. 2003CB716501) and the Key Laboratory of Lithospheric Tectonics and Exploration, China University of Geosciences, Ministry of Education of China (No. 2003015). Valuable comments and suggestions from Drs. Mungall, Roden and an anonymous reviewer and editorial handling of Professor Frederick A. Frey have dramatically improved the original manuscript and are highly appreciated. Thanks also to Ms. Ci Cai, Mr. Yongxing Zou, Mr. Shizhong Chen and Mr. Liwen Sun for their support in field work and CCSD sampling, and Ms. Ying Wang and Ms. Wenxia Zhao for their assistance with Laser Raman and electron probe analyses. Professor Rucheng Wang is appreciated for constructive discussions and suggestions.

REFERENCES

Anderssona U. B., Harlov D. E., Forster H. J., Nystrom J. O., Dulski P., and Bromand C. (2002) On the monazite inclusions in apatite from the Kiruna iron ores. *GFF* **124**, 232–233.

Arculus R. J. (1994) Aspects of magma genesis in arcs. *Lithos* **33**, 189–208.

Ballhaus C. (1993) Oxidation states of the lithospheric and asthenospheric upper mantle. *Contrib. Mineral Petrol.* **114**, 331–348.

Brandon A. D., and Draper D. S. (1996) Constraints on the origin of the oxidation state of mantle overlying subduction zones: an example from Simcoe, Washington, USA. *Geochim. Cosmochim. Acta* **60**, 1739–1749.

Carswell D. A., Wilson R. N., and Zhai M. (2000) Metamorphic evolution, mineral chemistry and thermobarometry of schists and orthogneisses hosting ultra-high pressure eclogites in the Dabieshan of central China. *Lithos* **52**(1–4), 121–155.

Cocherie A., and Albarede F. (2001) An improved U–Th–Pb age calculation for electronic microprobe dating of monazite. *Geochim. Cosmochim. Acta* **65**(24), 4509.

Corfu F. (1988) Differential response of U–Pb systems in coexisting accessory minerals, Winnipeg River Subprovince, Canadian Shield: implications for Archean crustal growth and stabilization. *Contrib. Mineral Petrol.* **98**(3), 312–325.

Hong J. A., Li S. G., William C. T., and Yang X. M. (2003) Needle-like exsolutions from apatite in ultrahigh-pressure eclogite and their genesis. *Acta Mineral. Sin.* **23**(3), 273–277 (in Chinese with English abstract).

Jin Z. M., Jin S. Y., Gao S., and Zhao W. X. (1998) Is the depth where UHP rocks formed in the Dabie Mountains limited to 100–150 km? *Chinese Sci. Bull.* **43**(1), 767–771 (in Chinese).

Li S., Jagoutz E., Chen Y., and Li Q. (2000) Sm–Nd and Rb–Sr isotopic chronology and cooling history of ultrahigh pressure metamorphic rocks and their country rocks at Shuanghe in the Dabie Mountains, central China. *Geochim. Cosmochim. Acta* **64**(6), 1077–1093.

Li S., Xiao Y., Liou D., Chen Y., Ge N., Zhang Z., Sun S.-s., Cong B., Zhang R., Hart S. R., and Wang S. (1993) Collision of the North China and Yangtse blocks and formation of coesite-bearing eclogites; timing and processes. *Chem. Geol.* **109**(1–4), 89–111.

Li S. G., and Sun W. D. (1996) A Middle Silurian Early Devonian magmatic arc in the Qinling Mountains of central China: a discussion. *J. Geol.* **104**(4), 501–503.

Li S. G., Sun W. D., Zhang G. W., Chen J. Y., and Yang Y. C. (1996) Chronology and geochemistry of metavolcanic rocks from Heigouxia valley in the Mian-Lue tectonic zone, south Qinling—evidence for a Paleozoic oceanic basin and its close time. *Sci. China D-Earth Sci.* **39**(3), 300–310.

Li Y. L., Zheng Y. F., and Fu B. (2001) An oxygen isotope study of quartz veins within eclogites from the Dabie terrane. *Sci. China (D)* **44**(7), 621–634.

Liang H.-Y., Campbell I. H., Allen C., Sun W.-D., Liu C.-Q., Yu H.-X., Xie Y.-W., and Zhang Y.-Q. (2006) Zircon Ce^{4+}/Ce^{3+} ratios and ages for Yulong ore-bearing porphyries in eastern Tibet. *Miner. Deposita* **41**, 152–159.

Liou J. G., and Zhang R. Y. (1996) Occurrences of intergranular coesite in ultrahigh-P rocks from the Sulu region, eastern China: implications for lack of fluid during exhumation. *Am. Mineral.* **81**(9–10), 1217–1221.

Liou J.G., Zhang R.Y., and Eide E.A. (1996) Metamorphism and tectonics of high-pressure and ultra-high-pressure belts in the Dabie–Sulu region, China. In *The Tectonics of Asia* (eds. M.T. Harrison and A. Yin). Cambridge Unviersity Press, pp. 300–344.

Liou J. G., Zhang R. Y., Ernst W. G., Rumble D., and Maruyama S. (1998) High-pressure minerals from deeply subducted metamorphic rocks. *Rev. Mineral.* **37**, 33–96.

Liu D. Y., Jian P., Kroner A., and Xu S. T. (2006a) Dating of prograde metamorphic events deciphered from episodic zircon growth in rocks of the Dabie–Sulu UHP complex, China. *Earth Planet. Sci. Lett.* **250**(3–4), 650–666.

Liu F. L., Gerdes A., Liou J. G., Xue H. M., and Liang F. H. (2006b) SHRIMP U–Pb zircon dating from Sulu–Dabie dolomitic marble, eastern China: constraints on prograde, ultrahigh-pressure and retrograde metamorphic ages. *J. Metamorph. Geol.* **24**(7), 569–589.

Luhr J. F., and Aranda-Gomez J. J. (1997) Mexican peridotite xenoliths and tectonic terranes: correlations among vent location, texture, temperature, pressure and oxygen fugacity. *J. Petrol.* **38**, 1075–1112.

Meng Q. R., and Zhang G. W. (2000) Geologic framework and tectonic evolution of the Qinling orogen, central China. *Tectonophysics* **323**(3–4), 183–196.

Montel J. M., Foret S., Veschambre M., Nicollet C., and Provost A. (1996) Electron microprobe dating of monazite. *Chem. Geol.* **131**(1–4), 37–53.

Mungall J. E. (2002) Roasting the mantle: slab melting and the genesis of major Au and Au-rich Cu deposits. *Geology* **30**(10), 915–918.

Parkinson I. J., and Arculus R. J. (1999) The redox state of subduction zones: insights from arc-peridotites. *Chem. Geol.* **160**, 409–423.

Parrish R. R. (1990) U–Pb dating of monazite and its application to geological problems. *Can. J. Earth Sci.* **27**(11), 1431–1450.

Rhede D., Wendt I., and Forster H. J. (1996) A three-dimensional method for calculating independent chemical U/Pb- and Th/Pb-ages of accessory minerals. *Chem. Geol.* **130**(3–4), 247–253.

Sillitoe R. H. (1997) Characteristics and controls of the largest porphyry copper–gold and epithermal gold deposits in the circum-Pacific region. *Aust. J. Earth Sci.* **44**(3), 373–388.

Sun, X. M., Xu, L., Zhai, W., Tang, Q., Liang, Y. H., Liang, J. L., Zhang, Z. M., and Shen, K. (2006) Nobel gases isotopic compositions of fluid inclusions in quartz veins and crystals collected from CCSD and Donghai HP-UHP metamorphic rocks. *Acta Petrol. Sin.* **22,** (7) 1999–2008 (in Chinese with English abstract).

Sun W. D., Arculus R. J., Kamenetsky V. S., and Binns R. A. (2004a) Release of gold-bearing fluids in convergent margin magmas prompted by magnetite crystallization. *Nature* **431**(7011), 975–978.

Sun W. D., Bennett V. C., and Kamenetsky V. S. (2004b) The mechanism of Re enrichment in arc magmas: evidence from Lau Basin basaltic glasses and primitive melt inclusions. *Earth Planet. Sci. Lett.* **222**(1), 101–114.

Sun W. D., Li S. G., Chen Y. D., and Li Y. J. (2002a) Timing of synorogenic granitoids in the South Qinling, central China: constraints on the evolution of the Qinling–Dabie orogenic belt. *J. Geol.* **110**, 457–468.

Sun W. D., Li S. G., Sun Y., Zhang G. W., and Li Q. L. (2002b) Mid-paleozoic collision in the north Qinling: Sm–Nd, Rb–Sr and $^{40}Ar/^{39}Ar$ ages and their tectonic implications. *J. Asian Earth Sci.* **21**(1), 69–76.

Sun W. D., Williams I. S., and Li S. G. (2002c) Carboniferous and Triassic eclogites in the western Dabie Mountians, east-central China: evidence for protracted convergence of the North and South China blocks. *J. Metamorph. Geol.* **20**, 873–886.

Suzuki K., and Adachi M. (1991) Precambrian provenance and silurian metamorphism of the Tsubonosawa paragneiss in the South Kitakami Terrane, Northeast Japan, revealed by the chemical Th-U-Total Pb isochron ages of monazite, zircon and xenotime. *Geochem. J.* **25**(5), 357–376.

Suzuki K., and Adachi M. (1994) Middle precambrian detrital monazite and zircon from the Hida Gneiss on Oki-Dogo Island, Japan—their origin and implications for the correlation of basement Gneiss of Southwest Japan and Korea. *Tectonophysics* **235**(3), 277–292.

Suzuki K., and Adachi M. (1998) Denudation history of the high T/P Ryoke metamorphic belt, southwest Japan: constraints from CHIME monazite ages of gneisses and granitoids. *J. Metamorph. Geol.* **16**(1), 23–37.

Williams I. S., Compston W., and Chappell B. W. (1983) Zircon and monazite U–Pb systems and histories of I-type magmas, Berridale Batholith, Australia. *J. Petrol.* **24**(1), 76–97.

Williams M. L., and Jercinovic M. J. (2002) Microprobe monazite geochronology: putting absolute time into microstructural analysis. *J. Struct. Geol.* **24**(6–7), 1013–1028.

Wood B. J., Bryndzia L. T., and Johnson K. E. (1990) Mantle oxidation state and its relationship to tectonic environment and fluid speciation. *Science* **248**, 337–345.

Xiao Y. L., Sun W. D., Hoefs J., Simon K., Zhang Z. M., Li S. G., and Hofmann A. W. (2006) Making continental crust through slab melting: constraints from niobium-tantalum fractionation in UHP metamorphic rutile. *Geochim. Cosmochim. Acta* **70**(18), 4770–4782.

Xu L., Sun X. M., Zhai W., Liang J. L., Liang Y. H., Shen K., Zhang Z. M., and Tang Q. (2005) Preliminary studies of fluid inclusions in quartz veins of HP-UHP metamorphic rocks, CCSD. *Acta Petrol. Sin.* **21**(2), 505–512 (in Chinese with English abstract).

Xu L., Sun X. M., Zhai W., Liang J. L., Liang Y. H., Shen K., Zhang Z. M., and Tang Q. (2006a) Fluid inclusions in quartz veins from HP-UHP metamorphic rocks, Chinese Continental Scientific Drilling (CCSD) project. *Int. Geol. Rev.* **48**(7), 639–649.

Xu L., Sun X. M., Zhai W., Liang Y. H., Tang Q., Liang J. L., and Shen K. (2006b) δD-δ18O compositions of fluid inclusions in quartz veins of HP-UHP rocks from the Chinese Continental Scientific Drilling (CCSD) project and its geological significances. *Acta Petrol. Sin.* **227**, 2009–2017 (in Chinese with English abstract).

Xu S. T., Okay A. I., Ji S. Y., Sengor A. M. C., Wen S., Liu Y. C., and Jiang L. L. (1992) Diamond from the Dabie-Shan metamorphic rocks and its implication for tectonic setting. *Science* **256**(5053), 80–82.

Xu Z. Q. (2004) The scientific goals and investigation progresses of the Chinese Continental Scientific Drilling Project. *Acta Petrol. Sin.* **20**(1), 1–8 (in Chinese with English abstract).

Xu Z. Q., Yang W. C., Zhang Z. M., and Yang T. N. (1998) Scientific significance and site-selection researches of the first Chinese Continental Scientific Deep Drillhole. *Cont. Dynam.* **3**, 1–13.

Yang J. J., and Jahn B. M. (2000) Deep subduction of mantle-derived garnet peridotites from the Su-Lu UHP metamorphic terrane in China. *J. Metamorph. Geol.* **18**(2), 167–180.

Ye K., Cong B. L., and Ye D. I. (2000) The possible subduction of continental material to depths greater than 200 km. *Nature* **407**(6805), 734–736.

Ye K., Liu J. B., Cong B. L., Ye D. N., Xu P., Omori S., and Maruyama S. (2002) Ultrahigh-pressure (UHP) low-Al titanites from carbonate-bearing rocks in Dabieshan-Sulu UHP terrane, eastern China. *Am. Mineral.* **87**(7), 875–881.

Zhai W., Sun X. M., Xu L., Zhang Z. M., Liang J. L., Liang Y. H., and Shen K. (2005) Fluid inclusions of Qinglongshan ultrahigh pressure metamorphic eclogite and fluid evolution, north Jiangsu province, China. *Acta Petrol. Sin.* **21**(2), 482–488.

Zhang G. W., Meng Q. G., Yu Z. P., Sun Y., Zhou D. W., and Guo A. L. (1996) Orogenesis and dynamics of the Qinling orogen. *Sci. China D-Earth Sci.* **39**(3), 225–234.

Zhang R. Y., and Liou J. G. (1999) Exsolution lamellae in minerals from ultrahigh-pressure rocks. *Int. Geol. Rev.* **41**(11), 981–993.

Zhang Z. M., Rumble D., Liou J. G., Xiao Y. L., and Gao Y. J. (2005a) Oxygen isotope geochemistry of rocks from the pre-pilot hole of the Chinese Continental Scientific Drilling Project (CCSD-PPH1). *Am. Mineral.* **90**(5–6), 857–863.

Zhang Z. M., Xiao Y. L., Liu F. L., Liou J. G., and Hoefs J. (2005b) Petrogenesis of UHP metamorphic rocks from Qinglongshan, southern Sulu, east-central China. *Lithos* **81**(1–4), 189–207.

Zhang Z. M., Xu Z. Q., Liu F. L., You Z. D., Shen K., Yang J. S., Li T. F., and Chen C. Z. (2004) Geochemistry of eclogites from the main hole (100 similar to 2050 m) of the Chinese Continental Scientific Drilling Project. *Acta Petrol. Sin.* **20**(1), 27–42.

Zhang Z. M., Zhang J. F., You Z. D., and Shen K. (2005c) Ultrahigh-pressure metamorphic P-T-t path of the Sulu orogenic eastern central China. *Acta Petrol. Sin.* **21**(2), 257–270.

Zheng Y. F. (2004) Fluids activities during the exhumation of deep-subducted continental plates. *Chinese Sci. Bull.* **49**(10), 917–929.

Zheng Y. F., Fu B., Gong B., and Li L. (2003) Stable isotope geochemistry of ultrahigh pressure metamorphic rocks from the Dabie–Sulu orogen in China: implications for geodynamics and fluid regime. *Earth-Sci. Rev.* **62**(1–2), 105–161.

Zheng Y. F., Wu Y. B., Chen F. K., Gong B., Li L., and Zhao Z. F. (2004) Zircon U–Pb and oxygen isotope evidence for a large-scale O-18 depletion event in igneous rocks during the neoproterozoic. *Geochim. Cosmochim. Acta* **68**(20), 4145–4165.

Zhu Y. F., and Massonne H. J. (2005) Discovery of pyrrhotite exsolution in apatite. *Acta Petrol. Sin.* **21**(2), 405–410.

Associate editor: Frederick A. Frey